Impact of an extreme melt event on the runoff and hydrology of a high Arctic glacier

Sarah Boon,[1]* Martin Sharp[1] and Peter Nienow[2]

[1] *Department of Earth & Atmospheric Sciences, University of Alberta, Edmonton, AB T6G 2E3, Canada*
[2] *Department of Geography & Topographic Science, University of Glasgow, Glasgow, UK*

Abstract:

On 28–30 July 2000, an extreme melt event was observed at John Evans Glacier (JEG), Ellesmere Island (79°40′N, 74°00′W). Hourly melt rates during this event fell in the upper 4% of the distribution of melt rates observed at the site during the period 1996–2000. Synoptic conditions during the event resulted in strong east-to-west flow over the northern sector of the Greenland Ice Sheet, with descending flow on the northwest side reaching Ellesmere Island. On JEG, wind speeds during the event averaged $8 \cdot 1$ m s^{-1} at 1183 m a.s.l., with hourly mean wind speeds peaking at $11 \cdot 6$ m s^{-1}. Air temperatures reached $8\,°C$, and rates of surface lowering measured by an ultrasonic depth gauge averaged 56 mm day^{-1}. Calculations with an energy balance model suggest that increased turbulent fluxes contributed to melt enhancement at all elevations on the glacier, while snow albedo feedback resulted in increased melting due to net radiation at higher elevations. The event was responsible for 30% of total summer melt at 1183 m a.s.l. and 15% at 850 m a.s.l. Conditions similar to those during the event occurred on only $0 \cdot 1$% of days in the period 1948–2000, but 61% of events occurred in the summer months and there was an apparent clustering of events in the 1950s and 1980s. Such events have the potential to impact significantly on runoff, mass balance and drainage system development at high Arctic glaciers, and changes in their incidence could play a role in determining how high Arctic glaciers respond to climate change and variability. Copyright © 2003 John Wiley & Sons, Ltd.

KEY WORDS   synoptic climatology; hydrometeorology; Canadian Arctic; extreme melt events; energy balance; ablation

INTRODUCTION

An extreme melt event occurred on John Evans Glacier (JEG), Ellesmere Island, Nunavut, Canada (Figure 1) in the period 28–30 July 2000. This event was characterized by significant increases in air temperature and wind speed, and by a concurrent decrease in relative humidity. Over the 3 days of the event, average rates of surface lowering at 1183 m a.s.l. increased significantly, from ∼13 mm day^{-1} to 56 mm day^{-1}, and supra- and pro-glacial discharges reached peak melt-season values. Rapid surface melting removed the cryoconite layer on the glacier surface. It thus appears that the event contributed disproportionately to summer ablation and runoff, and that it may have had a significant influence on the annual mass balance of the glacier. This raises the possibility that variations in the incidence of such events may contribute in a major way to inter-annual variability and longer-term changes in runoff and mass balance at high Arctic glaciers, where summer melt is typically very low.

To evaluate this possibility, this paper attempts to quantify the impact of the event on summer ablation and runoff. It also seeks to identify the synoptic conditions associated with the event, to determine the mechanisms by which melt was enhanced, and to evaluate the frequency with which such events have occurred within the period of instrumental record. Although several similar events have been recorded in the Canadian high Arctic (see Courtin and Labine, 1977; Doran *et al*., 1996), there has been no previous systematic study of their

---

* Correspondence to: Sarah Boon, Department of Earth & Atmospheric Sciences, University of Alberta, Edmonton, AB T6G 2E3, Canada.
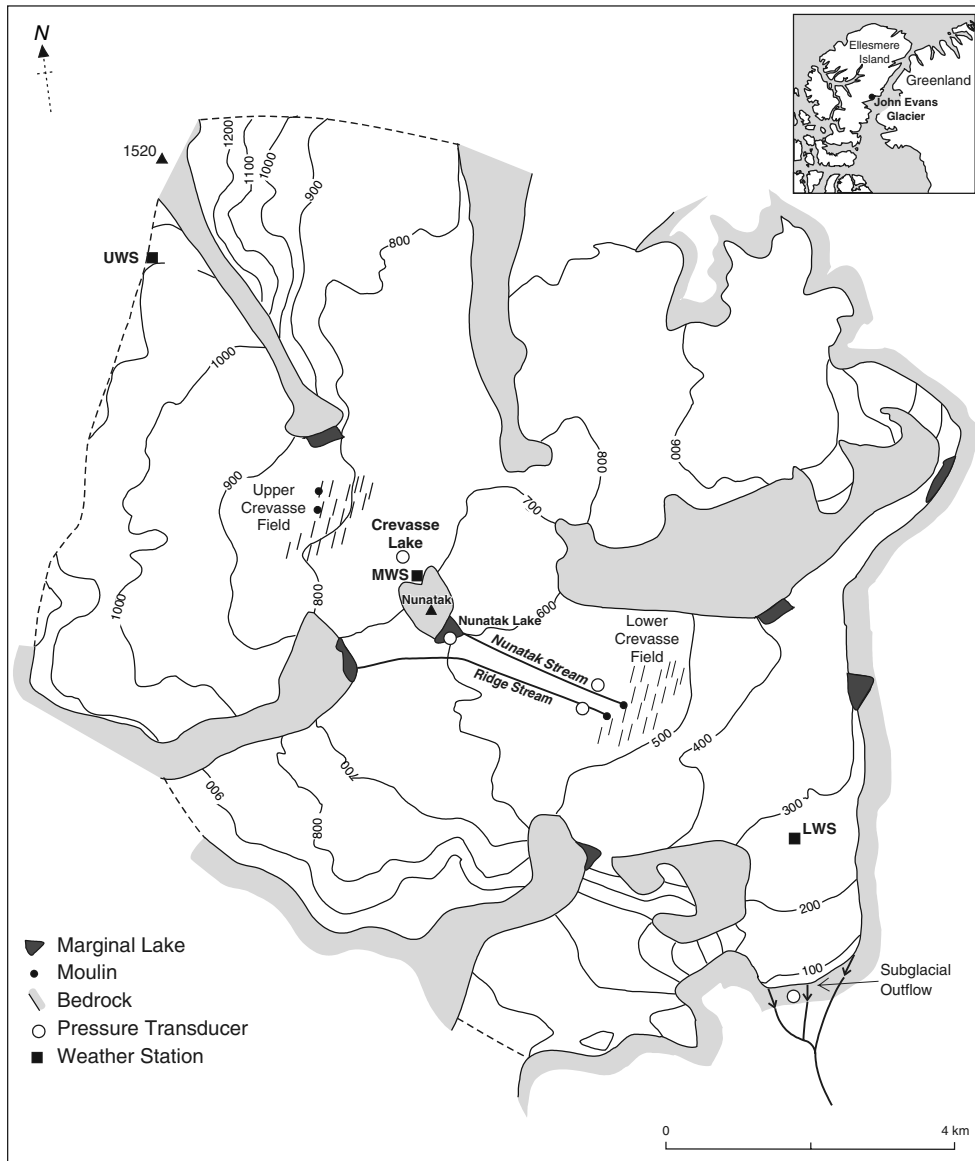E-mail: sboon@ualberta.ca

Figure 1. Site map of JEG. Inset map shows study site location; main map indicates location of meteorological and hydrological stations, and of supraglacial streams that connect to the englacial/subglacial drainage system via crevasses

incidence or impact on glacier runoff and mass balance. It has, however, been recognized that synoptically driven extreme melt events may be significant drivers for change in glacier hydrological systems (Gordon *et al*., 1998; Nienow *et al*., 1998).

STUDY SITE

JEG is a large valley glacier located at 79°40′N and 74°00′W, on the east coast of Ellesmere Island, Nunavut, Canada (Figure 1). It covers approximately 75% of a 220 km^2 catchment, with a length of 15 km and an

elevation range of 100–1500 m a.s.l. (Skidmore and Sharp, 1999). The glacier is polythermal, with cold-based ice in the accumulation area and at the glacier margins where ice is thin, and warm-based ice throughout the remainder of the ablation zone (Copland and Sharp, 2001). Ice thickness reaches a maximum of ∼400 m close to the equilibrium line, and 100–200 m in the lower 4 km of the glacier. During the period 1997–2000, mean annual air temperature at the equilibrium line (∼850 m a.s.l.) was −15·1 °C.

HYDROLOGY OF JEG

At the onset of summer melt, the drainage system of JEG consists of disconnected supraglacial lakes and streams, and there is no subglacial outflow. As surface melt progresses, snowmelt is routed both into storage in ice-marginal lakes and supraglacial channel systems (e.g. Nunatak and Ridge Lakes and Streams; Figure 1), and directly to ice-marginal streams. Eventually (late June to early July), the supraglacial Ridge and Nunatak Streams (and others in the same area) become connected to moulins located in a major crevasse field approximately 4 km from the glacier terminus (Lower Crevasse Field; Figure 1). The opening of these moulins allows water to drain from the surface to the glacier bed. Proglacial outflow of subglacially routed waters is usually initiated within 24 h of the moulins opening. Initially, outflow consists of extremely solute-rich waters that have probably been stored beneath the glacier over winter, but solute concentrations fall rapidly within 3 to 4 days as these 'old' waters are diluted by the new season's melt (Skidmore and Sharp, 1999; Heppenstall, 2001). Subglacial outflow emerges from one large portal at the centre of the glacier snout (Figure 1), but the resulting stream channel regularly changes course. In the cooler summers of 1994 and 1996, subglacial outflow occurred as a series of outburst floods, and the subglacial drainage system shut down between floods (Skidmore and Sharp, 1999). However, in the warmer summers of 1998–2000, outflow was continuous once initiated.

Most runoff that does not enter the Lower Crevasse Field is routed across the glacier surface to ice-marginal channels. In the summers of 1999–2001 (and possibly also in other summers), however, additional connections between surface channels and the en- and sub-glacial drainage systems developed at the Crevasse Lake and Upper Crevasse Field (Figure 1) later in the season, resulting in englacial/subglacial drainage of ∼40% of supraglacially derived meltwater.

METHODS

Synoptic conditions

Charts detailing synoptic conditions for 28–30 July 2000 were obtained from the National Center for Environmental Prediction's (NCEP) Climate Data Assimilation System (CDAS) daily reanalysis datasets (1000 mbar geopotential heights, and 1000 mbar zonal wind speed), and from the Meteorological Service of Canada (MSC) Northern Hemisphere daily analyses (500 mbar geopotential heights).

Local meteorological data

Meteorological data have been collected year-round at JEG since May 1996. Three on-ice automatic weather stations are deployed along the glacier centreline at 1183 m a.s.l. (upper weather station (UWS)), 824 m a.s.l. (middle weather station (MWS)) and 261 m a.s.l. (lower weather station (LWS)) (Figure 1). The LWS is located in the ablation zone, the MWS near the equilibrium line, and the UWS in the accumulation zone. During the summer melt season, hourly and daily averages of 10 s readings of air temperature, relative humidity (RH), net all-wavelength radiation Q^*, incoming and reflected solar radiation K_{in} and K_{out}, wind speed and direction, and rates of surface lowering are recorded at each station (Table I). The measurements of solar radiation include direct and diffuse components.

Table I. Meteorological station setup

Instrument	Location on Mast
LI200s Li-Cor pyranometer	Mast 1: on vertical pole on south end of crossarm, 1·80 m above snow, parallel to slope and pointed up
Kipp and Zonen pyranometer	Mast 1: on vertical pole on south end of crossarm, 0·8 m above snow, parallel to slope and pointed down
HMP 35CF Vaisala RH/temperature probe	Mast 1: housed in RM Young 12-plate Gill radiation shield (1·25 m)
RM Young 05103 wind monitor	Mast 1: on vertical pole on north end of crossarm (1·75 m above snow)
Vaisala PTB101 Barometric Pressure Sensor (*MWS only*)	Mast 1: in peli-case datalogger enclosure
REBS Q7 net radiometer	Mast 2: 0·80 m above snow, facing south
Campbell Scientific UDG01	Mast 2: 0·91 m above snow (*MWS*), 1·45m above snow (*UWS*); mounted at end of crossarm

Only data from the UWS and MWS are used in this study. Malfunction of the anemometer at the LWS precluded use of data from that station. Accurate measurements of surface lowering over the entire season (including the event) are available only from the UWS, as the masts supporting the ultrasonic depth gauges (UDGs) at both the MWS and LWS began to tilt during the melt event due to the high rates of surface lowering. Tilting also caused errors in Q^* values from the MWS for 28 July to 1 August. Data from 9 June–1 August were used in this study, as this is the period during which both meteorological stations were recording hourly average values. These data cover the majority of the melt season, which lasted from approximately 9 June to 10 August 2000.

The MWS was serviced four times during the field season. On each occasion, instrument heights were adjusted and masts were re-drilled. Owing to its distance from base camp, the UWS was serviced only twice: once at the beginning and once at the end of the field season. This is not considered problematic, as there was insufficient melt at this station to cause the masts to tilt. As net lowering at this site was <0·3 m over the whole season, no attempt is made to correct for the effect of changing instrument heights on melt calculations.

Melt calculations

Surface melt rates at the UWS and the MWS were calculated using the following energy balance equation:

$$Q_m = Q^* + \text{LHF} + \text{SHF} - \text{GHF} \tag{1}$$

where Q_m is the total energy available for melt, Q^* is the net radiation, LHF is the latent heat flux, SHF is the sensible heat flux, and GHF is the ground heat flux (Brock and Arnold, 2000). All terms were calculated in W m^{-2}, then converted to millimetres of water equivalent (mmWE) and summed to determine total melt at each meteorological station. Melt rates were output as both hourly and daily totals.

Calculations were performed using measured values of Q^*, and thus take account of diurnal variations in albedo, which are significant for melt at this latitude (Arendt, 1999). As the radiation sensors were aligned parallel to the slope, the effects of slope and aspect are also taken into account in the measured data. Erroneous Q^* values recorded at the MWS between 28 July and 1 August were replaced by Q^* values calculated using a point surface energy balance model (EBM) (Brock and Arnold, 2000). This model requires inputs of hourly values of air temperature, pressure and wind speed from a local meteorological station of known elevation, and a value for the aerodynamic roughness length at the point for which melt is being calculated. To calculate Q^*, the model required additional inputs of latitude, longitude, slope, aspect, elevation and albedo, as well as measured incoming solar radiation. The EBM assumes that: (1) cloud cover increases linearly as the ratio of measured K_{in} to theoretical clear-sky maximum K_{in} decreases; (2) the ice surface is constantly at 0 °C,

and energy is not required to return the surface to $0\,^\circ$C after a cold spell (which is likely incorrect for both sites at some points in the season); (3) vapour pressure just above the melting glacier surface is 611 Pa; and (4) the bulk aerodynamic method, incorporating the Monin–Obukhov similarity theory, is appropriate for this situation. When tested in an alpine setting, the model was found to approximate measured melt amounts very well, despite shading differences between the meteorological station and the modelled point (Brock and Arnold, 2000). In this study, melt is calculated only for those locations at which meteorological data are collected, and the effect of shading is taken into account by the measurements used to drive the model. For a more detailed description of the model, see Brock and Arnold (2000).

Comparison of hourly melt rates at the MWS, derived from both calculated and measured values of Q^*, shows that

$$Q_{m(calc)} = Q_{m(meas)} + 0.25 \text{ mmWE h}^{-1} \qquad (r^2 = 0.85) \tag{2}$$

for the period 9 June to 27 July, where $Q_{m(calc)}$ is melt determined using Q^* values calculated by the EBM, and $Q_{m(meas)}$ is melt determined using Q^* values measured at the meteorological station. Given the good relationship between the two values, substituting calculated for measured values during the period in question is justified. As calculated values are used for 5 days (28 July–1 August), melt during this period may be overestimated by as much as $\sim$30 mm.

The turbulent flux terms (LHF and SHF) were also calculated using the EBM. Positive LHF indicates energy being directed into the glacier surface (condensation). Negative LHF indicates energy being released from the glacier surface (evaporation/sublimation). At both the UWS and the MWS, SHF and LHF were calculated using data from 9 June to 1 August 2000 and the parameter values in Table II as model inputs. Owing to the uncertainty involved in assigning values for roughness length z_0, sensitivity tests were performed to determine the impact of varying z_0. Values for z_0 were obtained from Paterson (1994: 63), using measured albedo as a basis for characterizing surface conditions. The first sensitivity experiment involved comparing results from a simulation that used a constant value of z_0 for the entire melt season, with one that used different values of z_0 for sub-periods defined on the basis of observed variations in surface albedo. The constant value chosen was a weighted average of the values used for the different sub-periods. Given the possible error in the selection of z_0 values, a second constant z_0 experiment was performed using extreme high and low estimates of z_0 applied over the entire melt season. Tables III and IV list the z_0 values used in each sensitivity experiment.

Partitioning the melt season into sub-periods with different z_0 values resulted in only minor differences in predicted seasonal melt (3 mmWE and 8 mmWE at the MWS and UWS respectively) from the simulation using constant z_0. Differences in seasonal melt predictions using maximum and minimum estimates of z_0 are only 23 mmWE at the MWS and 15 mmWE at the UWS. Given the relatively small sensitivity of the EBM to variations in z_0, a single value for this parameter was used in subsequent simulations.

GHF was assigned a value of 17.6 W m^{-2} day^{-1} (based on the work of Konzelmann and Braithwaite (1995), in northeast Greenland), as heat conduction into the underlying ice is significant on non-temperate glaciers.

Table II. Input parameters for each run of the energy balance model

Parameter	MWS	UWS
Latitude	79·67	79·71
Longitude	−74·35	−74·56
Reference longitude	−75	−75
Summertime (h)	1	1
Elevation (m)	824	1183
Roughness length (m)	0·001	0·0005
Met station elevation (m)	824	1183

Table III. Input parameters for the first roughness sensitivity test. Note that albedo values are shown only to indicate the basis for selected roughness values, and are not used in the model

MWS			UWS		
Sub-period (JD)	Albedo[a]	Roughness (m)	Sub-period (JD)	Albedo[a]	Roughness (m)
161–170	0·60	0·0007	161–170	0·79	0·00055
171–192	0·52	0·001	171–184	0·66	0·0008
193–194	0·76	0·0005	185–206	0·86	0·0001
195–202	0·62	0·00075	207–209	0·76	0·0005
203–209	0·54	0·001	210–214	0·56	0·001
210–214	0·42	0·002	Weighted avg		0·0005
Weighted avg		0·001			

[a] $\geq 0\cdot6$ = snow; $<0\cdot6$ = ice.

Table IV. Input parameters for second roughness sensitivity test. Note that albedo values are shown only to indicate the basis for selected roughness values, and are not used in the model

	MWS			UWS	
Sub-period (JD)	Albedo[a]	Roughness (m)	Sub-period (JD)	Albedo[a]	Roughness (m)
Maximum roughness values					
161–170	0·60	0·007	161–209	0·74	0·007
171–192	0·52	0·06	210–214	0·56	0·06
193–202	0·69	0·007	Weighted avg		0·012
203–214	0·48	0·06			
Weighted avg		0·041			
Minimum roughness values					
161–170	0·60	0·001	161–209	0·74	0·001
171–192	0·52	0·01	210–214	0·56	0·01
193–202	0·69	0·001	Weighted avg		0·002
203–214	0·48	0·01			
Weighted avg		0·007			

[a] $\geq 0\cdot6$ = snow; $<0\cdot6$ = ice.

It is important to note that on high Arctic glaciers not all melt (Q_m) goes directly to runoff. Refreezing of meltwater that percolates into the cold snowpack plays a large role in delaying runoff at the start of the season. In 2001, for example, the delay between the onset of melt and the onset of runoff was approximately 12 days on the lower glacier, and 24 days on the upper glacier (D. Lewis, personal communication). Reeh (1991) suggested that an amount of water equivalent to approximately 60% of the winter snowpack might refreeze before runoff begins. This value was therefore used to determine seasonal runoff from calculated melt. The initial snow water equivalent (SWE) at the start of the 2000 melt season was 83·8 mm at the MWS, and 93·8 mm at the UWS.

Total summer melt at the MWS and UWS was calculated by summing modelled daily melt totals. The proportion of summer *melt* that occurred during the extreme melt event was determined by dividing the total melt from 28–30 July by the seasonal total (9 June–1 August). The proportion of summer *runoff* contributed by the melt event was estimated by dividing the total melt from 28–30 July by the estimated total runoff (total melt minus 60% of initial SWE at each weather station).

Glacier hydrology

Water levels in supraglacial streams were monitored throughout the melt season. Keller 169-L pressure transducers connected to Campbell Scientific CR10 dataloggers were placed in the Nunatak Lake, Ridge Stream, and Crevasse Lake (Figure 1). Relative stage values were recorded every 10 s, and an average reading was output every 15 min. Owing to frequent channel aggradation and migration, the record from a transducer placed in the proglacial stream was unreliable. Observations of proglacial drainage system development over the melt season were therefore also used to assess changes in runoff qualitatively. Proglacial discharge volumes were estimated to reach $\sim$30 m^3 s^{-1} during the melt event, but reliable measurements were difficult to obtain by the velocity–area method when discharge was in excess of $\sim$5 m^3 s^{-1}.

Past events

Frequency distributions of mean daily summer (June, July, August (JJA)) air temperature, wind speed, and relative humidity, were derived from the 5 year JEG climate record (1996–2000) to determine where the days of the melt event fall within these distributions. In addition, a 50 year record of daily synoptic conditions (Keimig, unpublished results) was searched to determine the frequency of occurrence of days with synoptic conditions similar to those associated with the event. The database constitutes a 7×28 grid (seven grid points of latitude by 28 grid points of longitude), spanning 90–75 °N and 110–42·5 °W. The size of each grid box is $2·5° \times 2·5°$.

RESULTS

Synoptic conditions

MSC 500 mbar geopotential height maps for the period of the melt event show a low over northwest Greenland that deepened and moved into Baffin Bay. A stationary low was located over the Barents Sea, a weak high was located over the Arctic Ocean, and a second high was moving northwards from the Queen Elizabeth Islands (Figure 2). This high reached its most northerly position on 29 July. By the end of 30 July it had disappeared, and the low over Greenland had moved southwestwards, over Baffin Island.

NCEP 1000 mbar height maps show a weak low over western Greenland, which intensified during the course of the event (28–30 July) to encompass most of Baffin Bay (Figure 3). NCEP 1000 mbar zonal wind charts show an area of peak wind strength over northwest Greenland, extending into central Ellesmere Island (Figure 4).

Local meteorology

The onset of the melt event was marked by a shift in wind direction to northeast at 1:00 h on 28 July (Figure 5). This shift was recorded at both the MWS and the UWS, suggesting that it dominated over local wind patterns, which vary greatly between stations throughout the melt season. At each station, the shift in wind direction was accompanied by an $\sim$5 m s^{-1} increase in wind speed, and a 3–5 °C increase in air temperature (Figures 5 and 6). Initially, RH dropped to 45% at each station, but by 29 July it had returned to background values of 70–75% (Figure 6). Wind speeds reached a maximum of 13·5 m s^{-1} at the MWS and 11·5 m s^{-1} at the UWS; air temperatures peaked at 10 °C at the MWS and 8 °C at the UWS, and remained high overnight, displaying only weak diurnal variation. By 30 July, winds at the MWS had shifted to the north–northwest, and wind speeds had diminished. By 31 July, the air temperature had returned to seasonal background values. Winds at the UWS did not return to north–northwest until 12·00 h on 1 August.

UDG measurements at the UWS indicate surface lowering rates of 80 mm day^{-1} on 28 July, with lower rates of 57 mm day^{-1} and 30 mm day^{-1} on 29 and 30 July respectively, giving an average lowering rate of 56 mm day^{-1} over the period of the event (Figure 7). These were the highest rates recorded during the melt
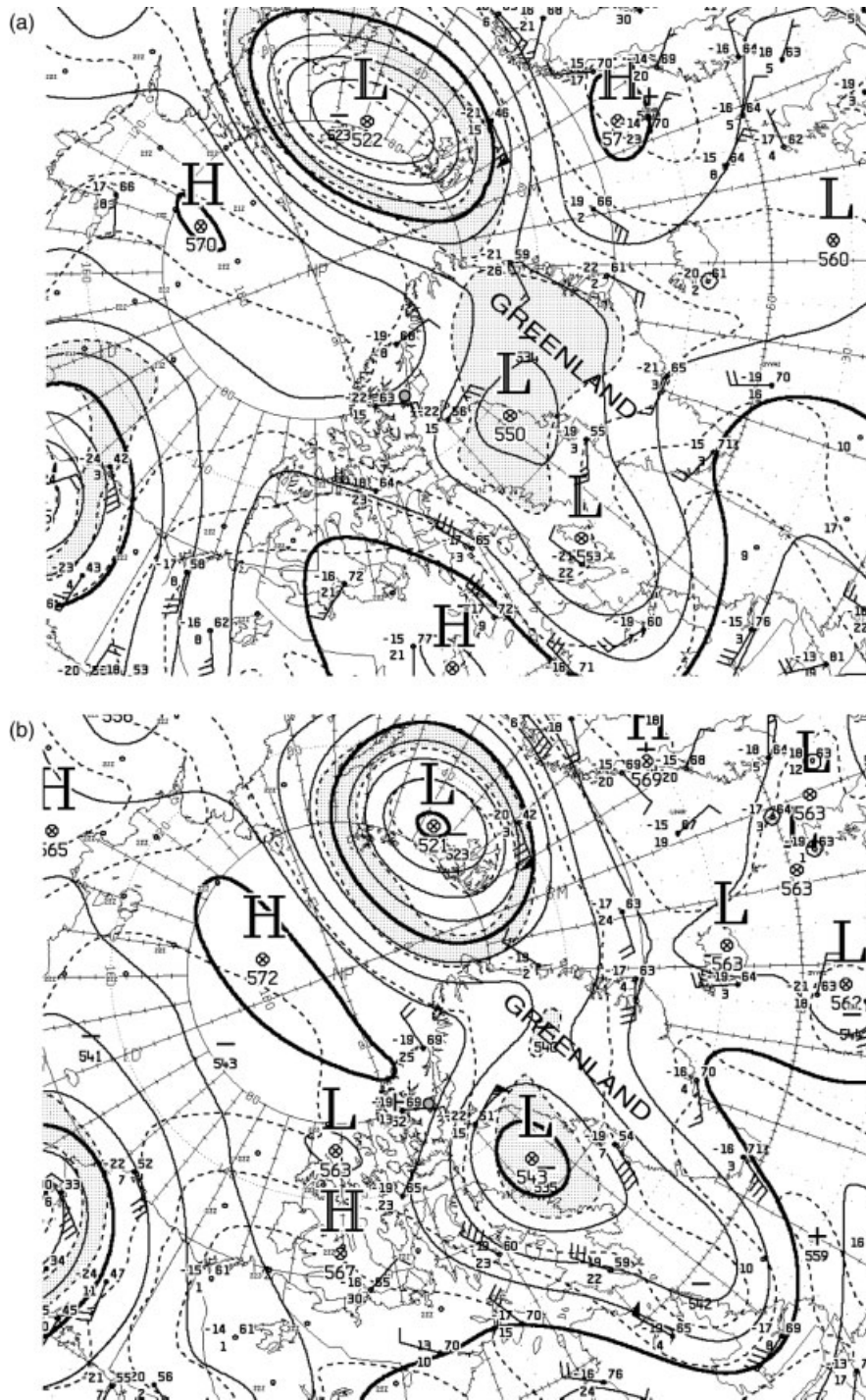
Figure 2. 500 mbar geopotential heights on (a) 28 July and (b) 29 July 2000 from the Meteorological Service of Canada. Greenland is labelled; JEG is marked with a dot
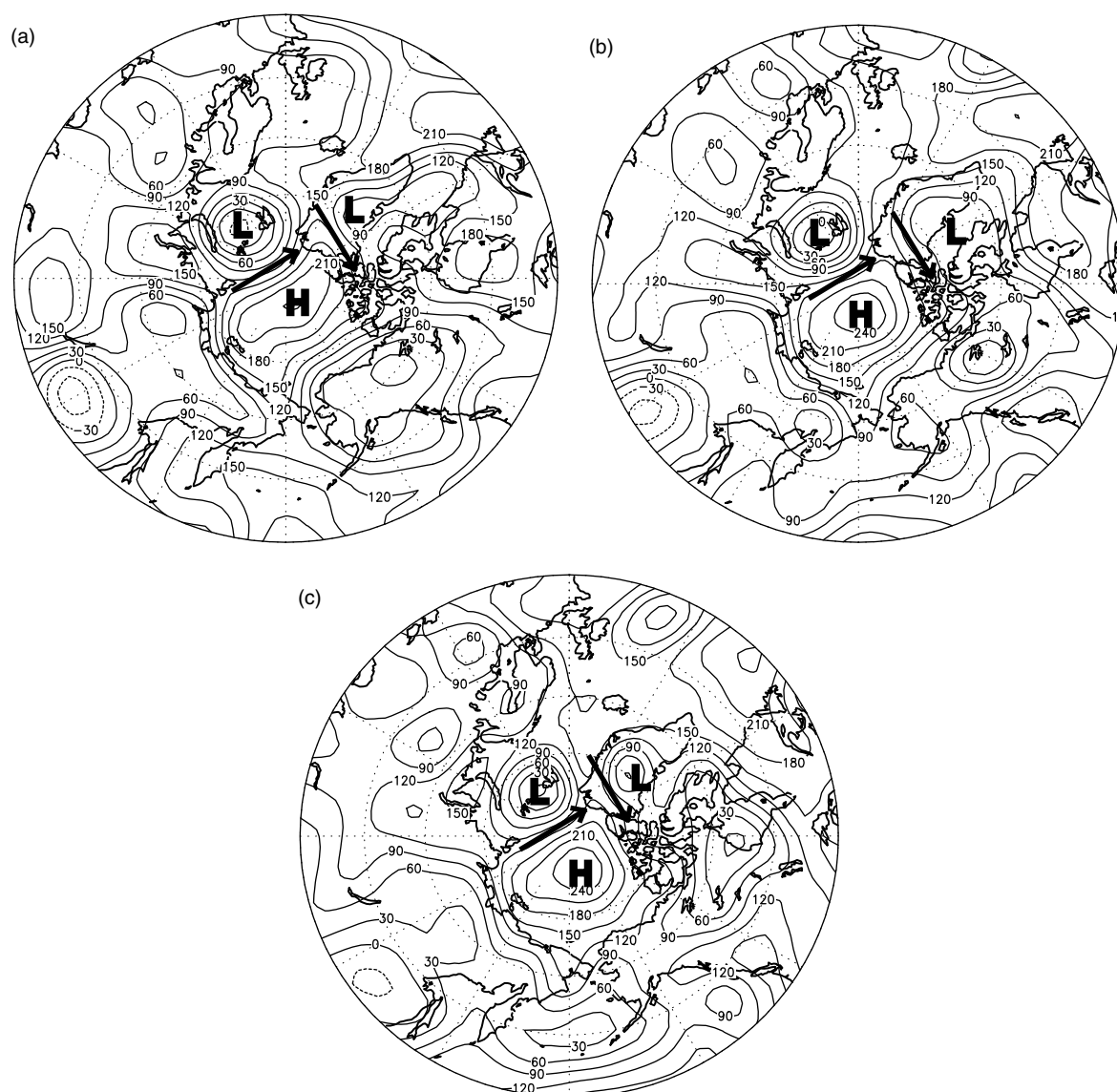
Figure 3. 1000 mbar geopotential heights on (a) 28 July, (b) 29 July, and (c) 30 July 2000 from the NCEP reanalysis. Pressure centres are labelled: L = low, H = high; direction of flow is marked by the arrows

season, and are significantly higher than the 13 mm day^{-1} average for the 3 days immediately prior to the event (24–27 July).

Verification of EBM output

The UDG data were collected over a melting snow surface. Since the density of the melting snow is unknown, the UDG data cannot be used for quantitative validation of the performance of the EBM. Since internal re-freezing of initial melt causes snowpack densification, rather than runoff, the calculated melt likely exceeds the amount of water actually removed from the snowpack. In addition, the effects of summer
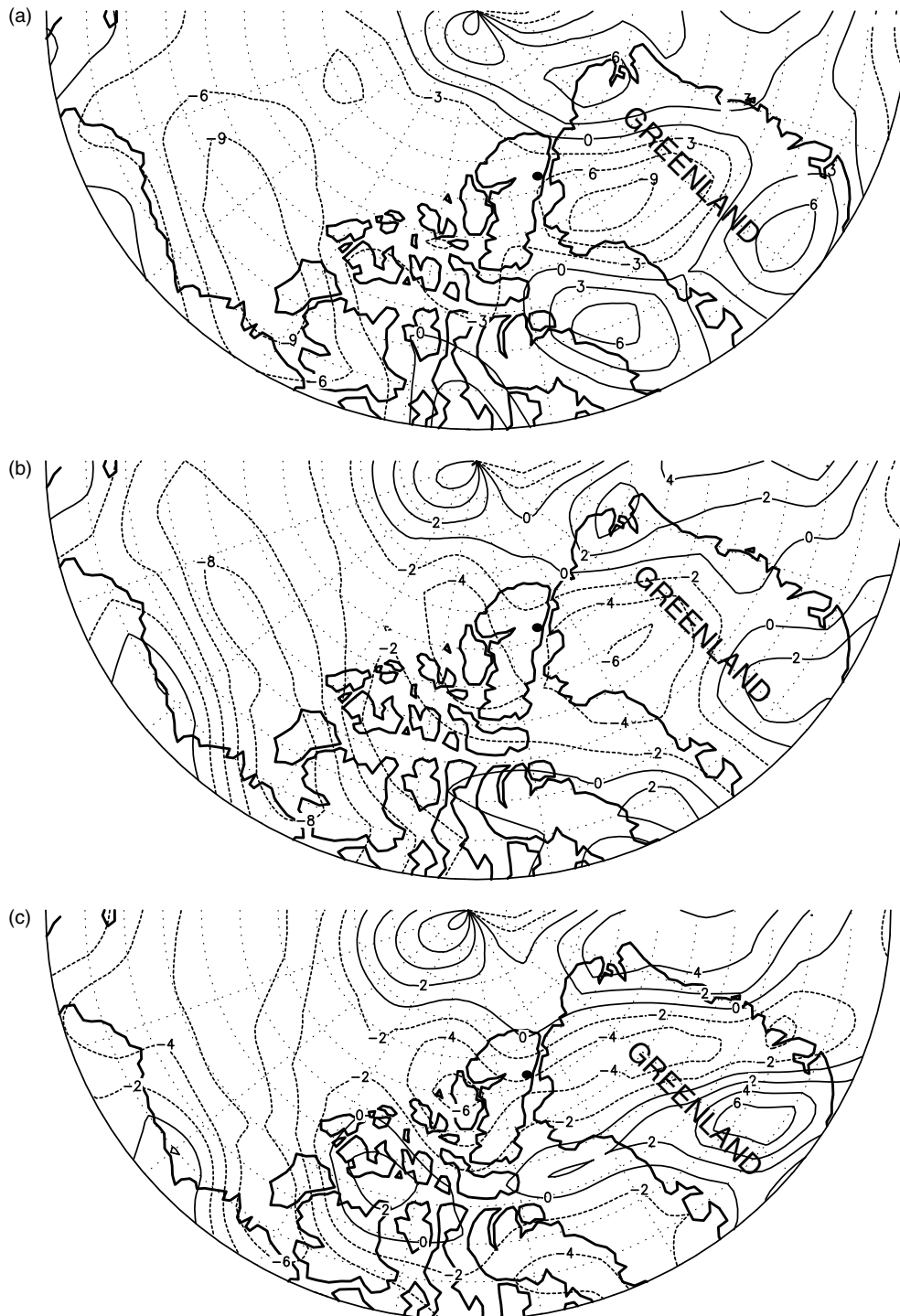
Figure 4. Surface u (E−W component of the wind) wind speed (m s^{-1}) on (a) 28 July, (b) 29 July, and (c) 30 July 2000 from the NCEP reanalysis. Negative values indicate easterly winds; positive values indicate westerly winds. Greenland is labelled; JEG is marked with a dot
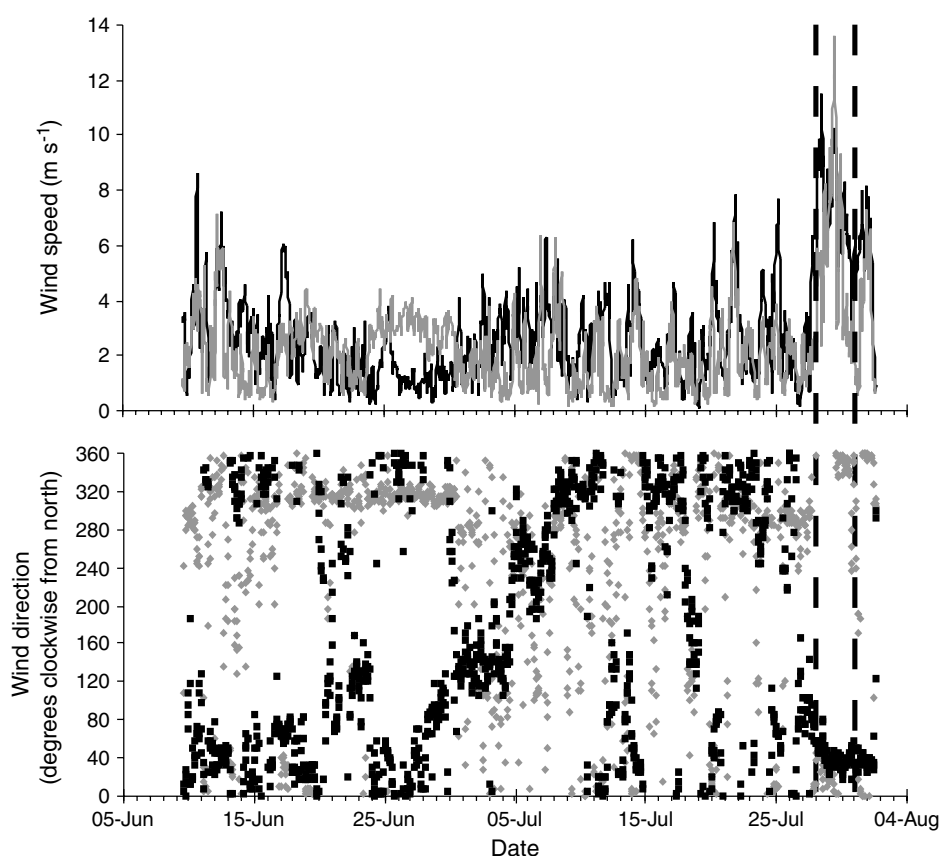
Figure 5. Wind speed (m s^{-1}) and direction at the MWS (grey) and the UWS (black). The dashed lines mark the period of the event

snowfalls, which raise surface elevation, are not included in the model simulations, as accurate measurements of snowfall amounts and densities are not available.

Despite these limitations, there is good qualitative correspondence between the EBM calculations and recorded rates of surface lowering at both stations (Figure 8). EBM output captures the main periods of high and low lowering rate detected by the UDG, and the significant difference in total lowering between the two sites. Calculated early-season melt is mirrored by a gradual decrease in surface height at both sites. Low calculated melt during a relatively cool period in early–mid July coincides with a period of surface height increases due to snowfall. The extreme melt event is marked by a sudden increase in calculated melt, and a corresponding rapid decline in surface height at the UWS.

Total melt at the UWS over the melt season was calculated as 404 mm WE, and total surface lowering recorded by the UDG was approximately 350 mm. At the MWS, the UDG and EBM records correspond well until the period of the melt event (after which the UDG record is unreliable due to tilting of the mast). Total melt calculated by the EBM between 9 June and 27 July was approximately 711 mm WE, and the total surface lowering in this time period was 560 mm. This reflects the differences between the UDG and the EBM records outlined above.

Surface energy balance

During the melt event, Q^* and SHF were the most significant energy sources at both the MWS and the UWS, whereas LHF was less important. LHF was, however, a strong source of melt energy during the
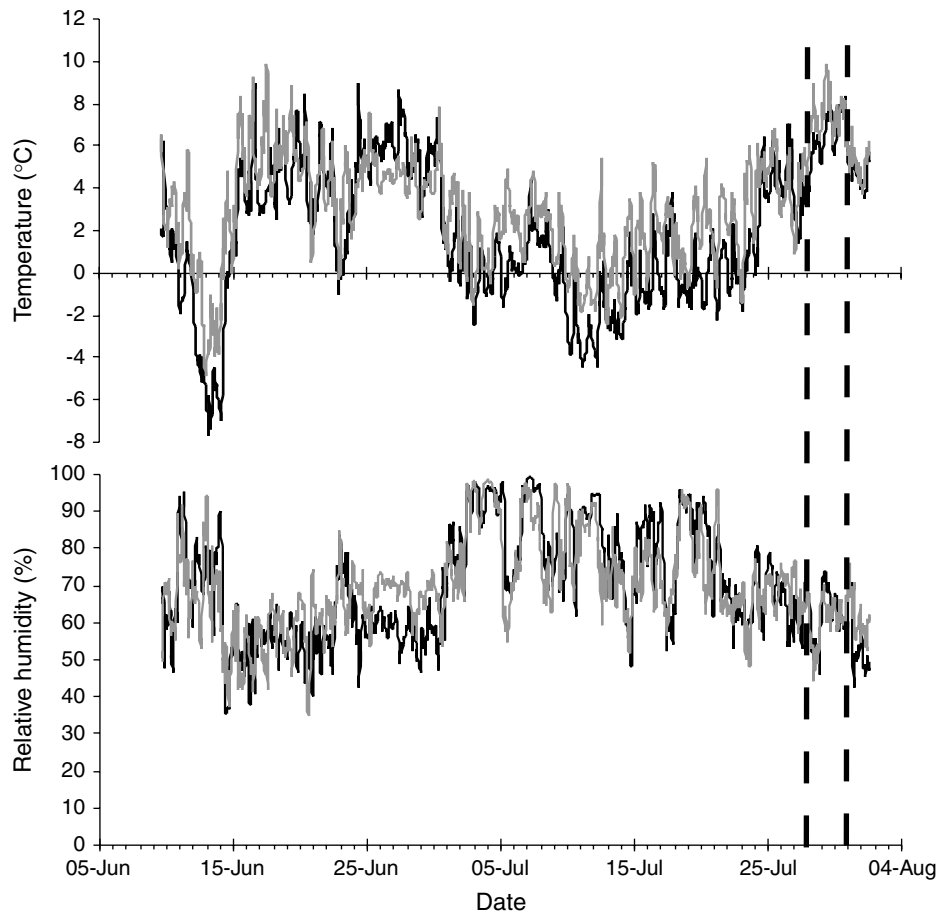
Figure 6. Temperature (°C) and relative humidity (%) at the MWS (grey) and the UWS (black). The dashed lines mark the period of the event

latter part of the event, as opposed to the energy sink it represented for the remainder of the melt season (Figure 9).

At the MWS, values of $Q*$ during the melt event were similar to those reached under clear sky conditions earlier in the summer. At the UWS, $Q*$ reached a seasonal peak during the event. SHF, though positive for most of the melt season, increased significantly during the event, from <0.5 mm WE h^{-1} to 3 mm WE h^{-1} at the MWS, and to 1·6 mm WE h^{-1} at the UWS (Figure 9). The period of high SHF lasted longer at the UWS than the MWS, however. SHF returned to seasonal background values by 31 July at the MWS, and a day later at the UWS. At both the MWS and the UWS, LHF became strongly negative on 28 July, and then switched to strongly positive on 29 July (Figure 9). It remained positive until 31 July. During most of the remainder of the season, LHF was negative, except during a rainy period on 7 July. Although LHF at the onset of the event was more negative at the UWS than at the MWS, it reached a similar maximum at both stations ($\sim$0·4 and 0·6 mm WE h^{-1}) during the event.

Melt rates

Hourly melt rates at both stations were commonly <0.5 mm WE h^{-1} (Figure 10). Such rates occurred 55% of the time at the MWS, and 74% of the time at the UWS. By contrast, melt rates during the event reached
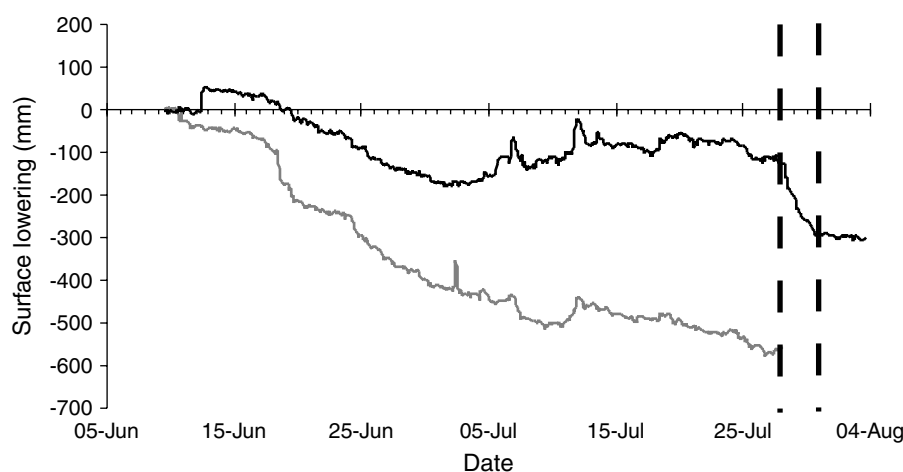
Figure 7. UDG records of surface lowering (mm) at the MWS (grey) and the UWS (black). The dashed lines mark the period of the event

$6 \cdot 1$ mm WE h^{-1} at the MWS, and $3 \cdot 7$ mm WE h^{-1} at the UWS, values which lie above the 96th percentile of the melt rate distribution for the season.

The melt event (28–30 July) was responsible for 17% and 30% of total seasonal *melt* at the MWS and UWS respectively, even though the event occupied only 6% of the melt season (Figure 11). Assuming that an amount of melt equivalent to 60% of the winter snowpack refroze within the snowpack (Reeh, 1991), the contribution of the event to total seasonal *runoff* is estimated as approximately 18% at the MWS and 35% at the UWS. Since runoff is equivalent to summer ablation, these results underline the potential impact of events such as this on the mass balance of glaciers in the Canadian high Arctic, where ablation totals are low and inter-annual variability in mass balance is largely attributable to variations in summer balance (Paterson, 1994).

Hydrological records

High melt rates during the event produced a clear response in the pressure transducer records from the Nunatak Lake and Ridge Stream, which experienced the second-highest water levels of the season during this period (Figure 12). In the Nunatak Lake, stage was higher only at the beginning of the season, before the lake connected to the supraglacial drainage system. In the Ridge Stream, peak water levels earlier in the season resulted from the drainage of the Ridge Lake, which occurred after a connection was established between the Ridge Stream and the englacial/subglacial system.

Water levels in the Nunatak Lake began to increase rapidly on 28 July, rising 3 m in 24 h to peak at 3·5 m on 29 July. The amplitude of this rise was at least five times that of the normal daily stage cycle during the pre-event period. In the Ridge Stream, water levels also increased on 28 July, rising 0·5 m in 36 h to peak at 0·8 m on 29 July. This rise was approximately 1·5 times the normal daily rise during the pre-event period. Although water level in the Crevasse Lake had been decreasing steadily in the days prior to the event, it increased rapidly by ∼0·5 m on 29 July, before beginning to drop again. As melt rates remained high throughout the night, the normal diurnal runoff cycle was overridden and water levels remained high overnight, only dropping to values typical of daily minima during the pre-event period on the final day of the melt event. The Crevasse Lake drained abruptly 2 days after the extreme melt event.

Numerous observations confirm that the high melt rates during the event resulted in large volumes of water being routed through the englacial/subglacial drainage system. The surface layer of the glacier, in which cryoconite holes up to 0·2 m in depth were developed, was removed by melting, and the resulting bare ice surface was covered with a thin film of water. Water exiting the glacier covered a significantly larger area of the
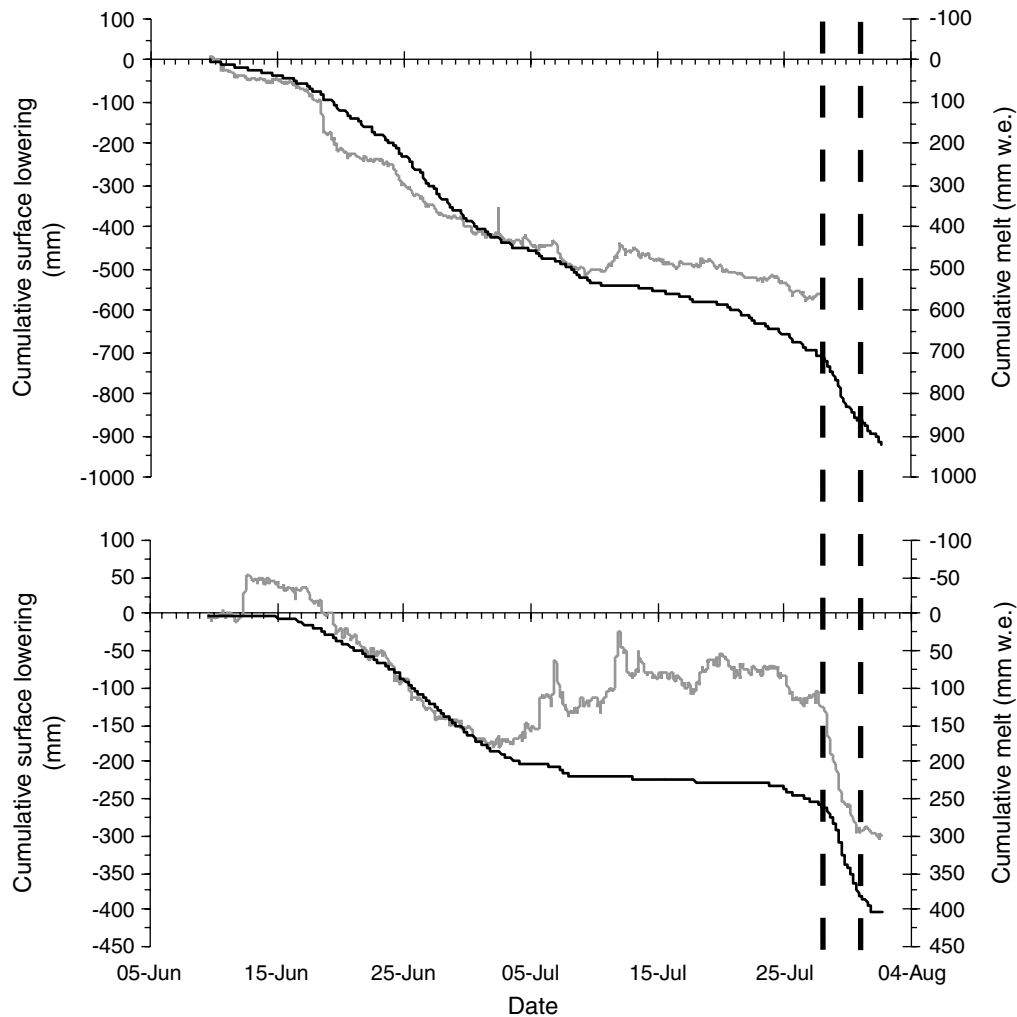
Figure 8. Surface lowering (grey) and calculated cumulative melt (black) at the (a) MWS and (b) UWS. The dashed lines mark the period of the event

proglacial outwash plain than in the pre-event period. A standing wave ~1 m high appeared 5 m downstream from the proglacial outlet, and boulders up to 50 cm in diameter were entrained during peak discharge.

Historical climate record

Except in 2000, daily mean air temperatures greater than 8 °C were not recorded at either the MWS or the UWS during the 5 years of record (Figure 13). Thus, conditions during the event constitute the 100th percentile of the air temperature distribution. Wind speeds greater than 5 m s^{-1} at the MWS are in the 98th percentile of the distribution, whereas at the UWS they are in the 97th percentile. RH lower than 45% is in the 99·96th percentile at the MWS, and the 90th percentile at the UWS. Further examination of the local meteorological record indicates that the specific combination of conditions that occurred during the event (high wind speed, high air temperature, and reduced relative humidity) did not occur at JEG on any other occasion in the period 1996–2000.
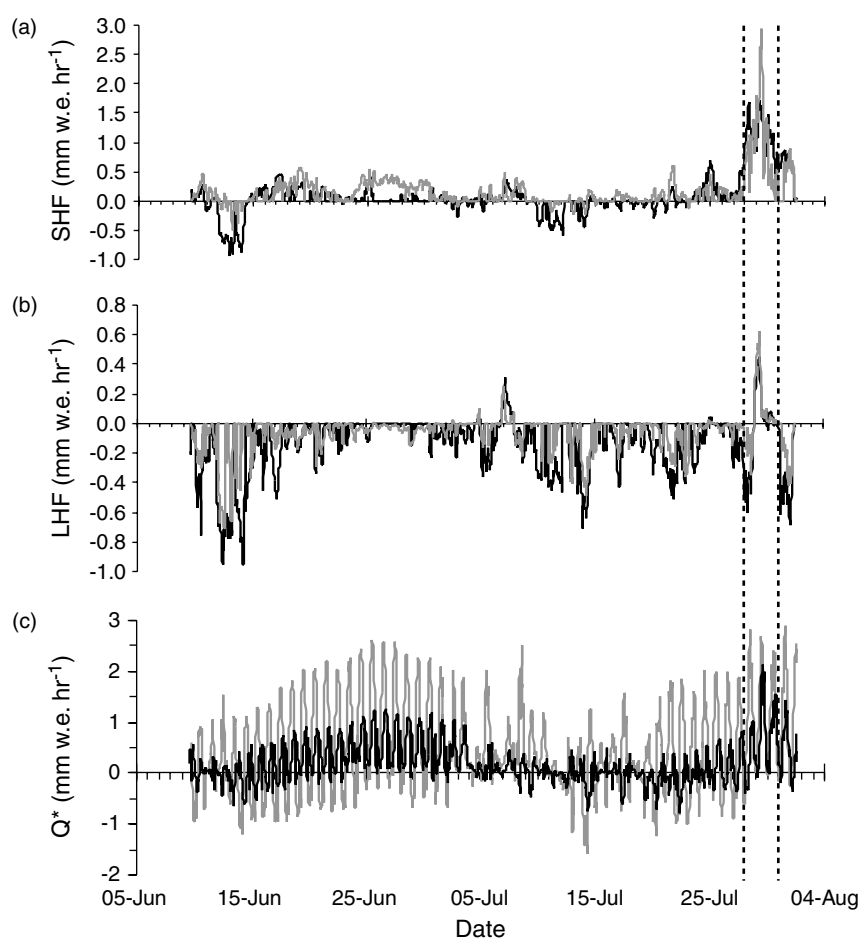
Figure 9. Contributions of (a) SHF, (b) LHF, and (c) Q^* to melt at the MWS (grey) and the UWS (black). The dashed lines mark the period of the event

A search of Keimig's (unpublished) synoptic database indicates that conditions similar to these occurred on only 0·1% of days between 1948 and 2000. Some 61% of days with these synoptic conditions occurred during the summer season (JJA), with the majority occurring in June and July (Figure 14). The year 1987 had the greatest number of days with similar conditions, and many years had none at all (Figure 15). Occurrence of similar synoptic conditions was generally highest during the 1950s and 1980s, and low during the 1960s, 1970s and 1990s.

DISCUSSION

Synoptic, meteorological and energy balance conditions

The synoptic conditions during the period 28–30 July 2000 created a large-scale pressure gradient between the low over northwest Greenland and the high over the Arctic Ocean, forcing air to rise orographically over the northeastern region of the Greenland Ice Sheet. The descent of this air on the lee (northwest) side of the ice sheet likely led to adiabatic warming, causing the resulting northeast winds to feed warm air into the
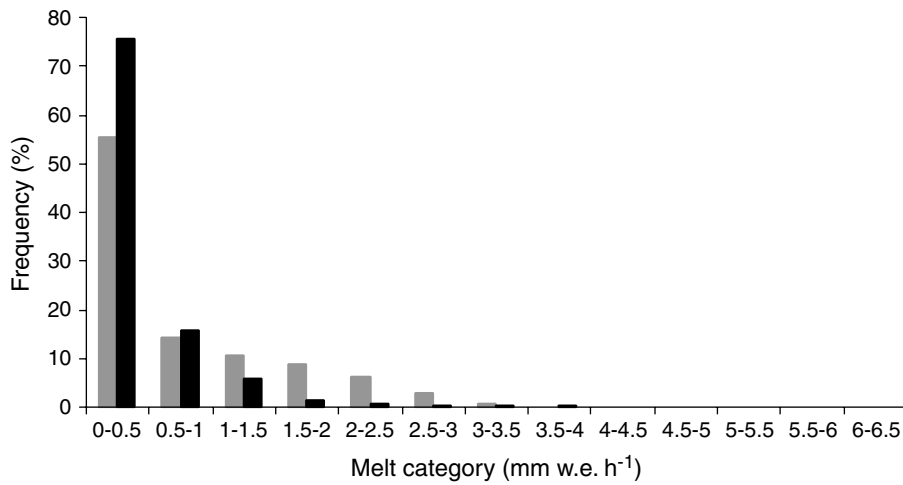
Figure 10. Frequency distribution of calculated hourly melt amounts in 2000 for the MWS (grey) and the UWS (black)
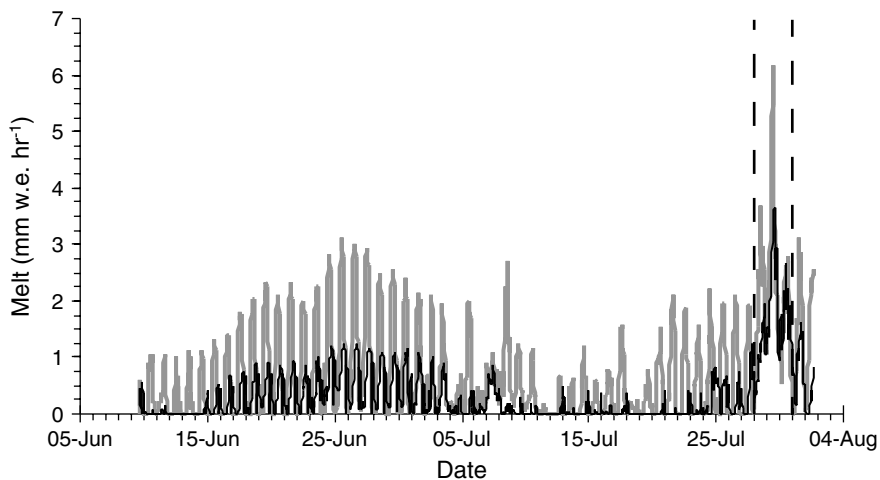

Figure 11. Calculated total-season melt at the MWS (grey) and the UWS (black). The dashed lines mark the period of the event

study area (Barry, 1992). This is indicated by the shift in wind direction to the northwest at both the UWS and MWS, as well as by the increases in air temperature and wind speed.

EBM results indicate an increase in sensible heat transfer at the onset of the event, as warm air was advected into the study area. The initial increase in SHF, however, was partly offset by the strongly negative LHF, which directed melt energy out of the glacier surface through evaporation/sublimation. The equilibration of the melting surface with the overlying atmosphere, which is indicated by the return of RH to background values, resulted in a positive peak in LHF, and peak melt rates on 29 July.

Differences between stations

The differences in the relative contributions to melt of each energy balance component, especially Q^*, between the MWS and the UWS suggest that altitude has a significant impact. Air temperatures at the UWS are generally lower than at the MWS, especially during periods of colder weather (Figure 6). Surface albedo is also higher at the UWS, as melt rates are lower and summer snowfalls are more frequent than at the MWS
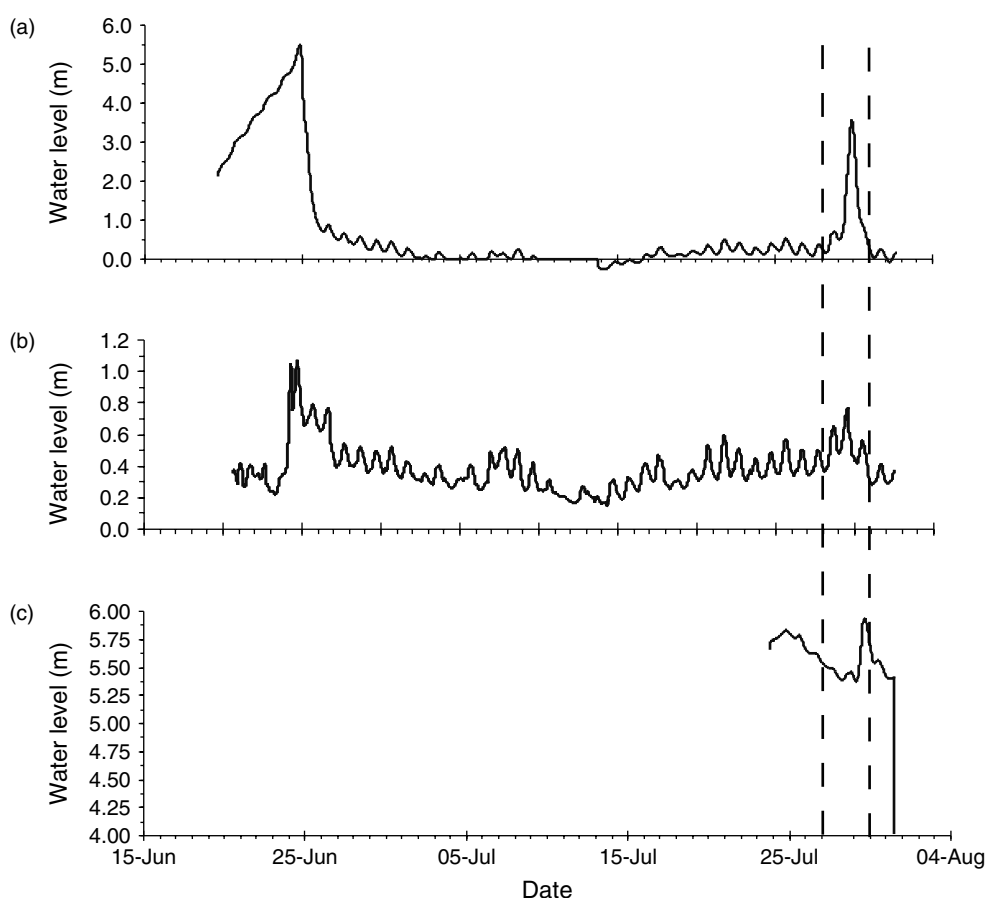
Figure 12. Water level (transducer) records from the (a) Nunatak Lake, (b) Ridge Stream, and (c) Crevasse Lake. The dashed lines mark the period of the event

(Figure 16). Air temperatures at the UWS remained close to $0\,°C$ for a period of ~ 2 weeks in early to mid-July. Albedo thus remained high following fresh snowfalls in early July (Figure 16), as there was insufficient energy to produce melt (Figure 9c). During the melt event, however, melt driven initially by increases in Q^* and SHF lowered the surface albedo sufficiently through alteration of snowpack properties so that Q^* made a large contribution to melt generation later in the event, when LHF was also a source of melt energy (Figures 9 and 16).

At the MWS, however, air temperatures remained above freezing through most of July (Figure 6) and melt occurred through most of this period (Figure 7). This was driven largely by Q^*, with a small and intermittent contribution from SHF. Snowfall around 12 July was less significant than at UWS (Figure 8), and although it resulted in a short-term increase in albedo (Figure 16), this was quickly reversed when melt resumed. As a result, surface albedo was lower for most of the season than at UWS (Figure 16), and the enhancement of Q^* by snow-albedo feedback during the melt event was less marked than at UWS. Thus, the relative importance of the extreme event at MWS (17% of seasonal melt) was less than at UWS (30% of seasonal melt).

Implications for glacier hydrology

The event described above occurred relatively late in the melt season at JEG, when drainage connections had been established between the glacier surface and glacier bed, and outflow of subglacially routed runoff
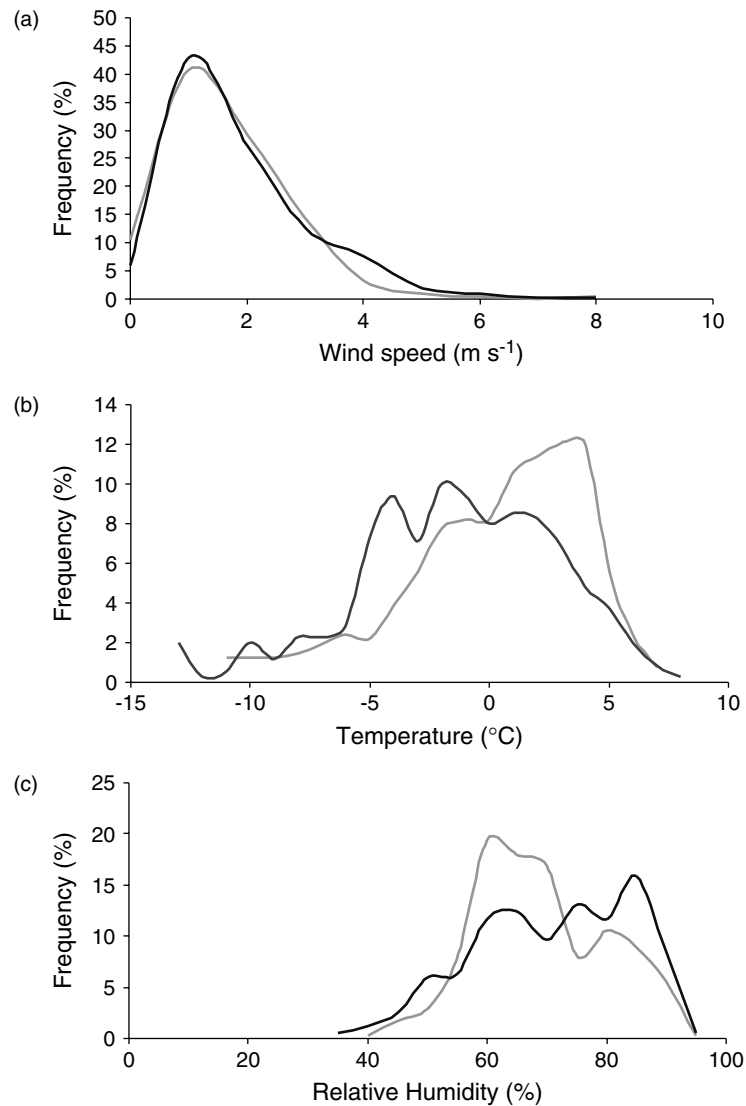
Figure 13. Frequency distribution of (a) wind speed, (b) temperature, and (c) relative humidity, calculated from MWS (grey) and UWS (black) data collected at the study site between 1996 and 2000

had begun. Although the event made a very significant contribution to total surface melt and runoff in the 2000 melt season, it probably did not play a major role in the seasonal development of the glacier drainage system. Keimig's (unpublished) synoptic analysis, however, shows that conditions similar to those that created the melt event occur most frequently in June, July and August, i.e. throughout the summer melt season (Figure 14). It thus seems likely that the nature and magnitude of the impact of such events may vary depending on the stage of the melt season at which they occur.

Several workers have suggested that such extreme runoff events could have a significant impact on subglacial drainage system development (Gordon *et al*., 1998, Nienow *et al*., 1998). At JEG, the major event in the seasonal development of the glacier's drainage system is the establishment of a drainage connection between the glacier surface and glacier bed, and the ensuing initiation of subglacial outflow. During the period
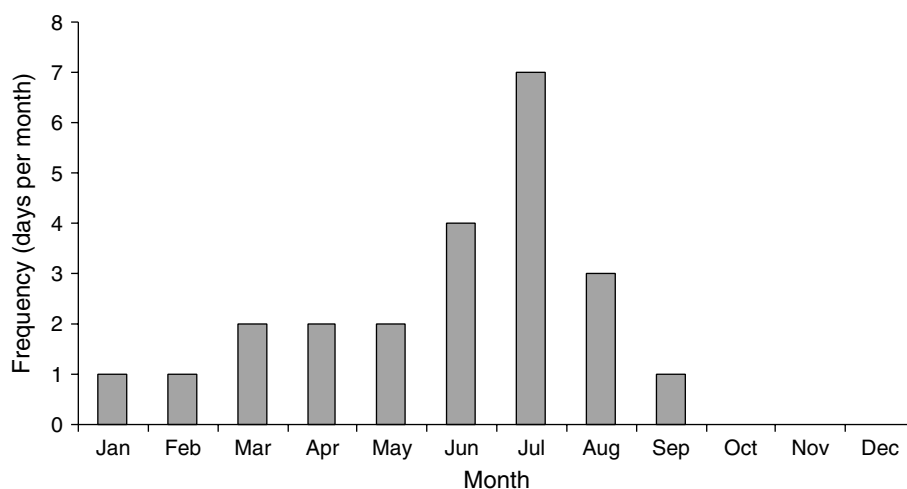
Figure 14. Monthly frequency distribution of synoptic conditions, similar to those that generated the extreme melt event, for the period 1948–2001, based on Keimig's (unpublished data) synoptic classification
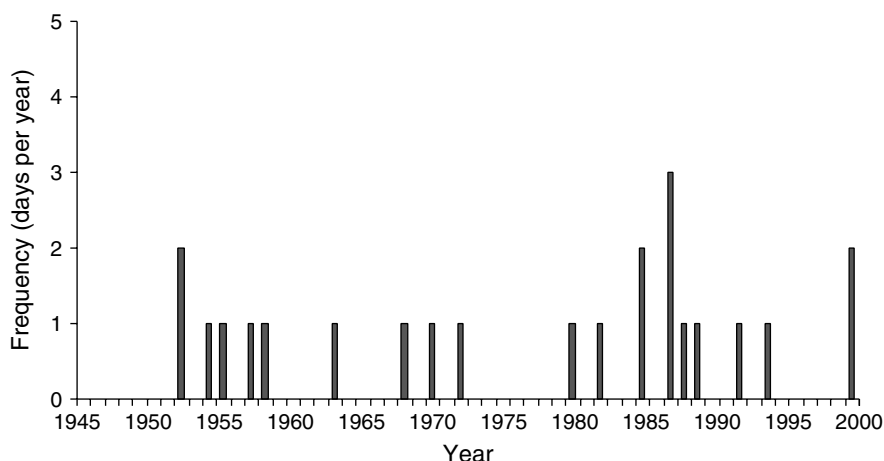

Figure 15. Annual frequency distribution of synoptic conditions, similar to those that generated the extreme melt event, for the period 1948–2001, based on Keimig's (unpublished data) synoptic classification

1994–2001, this event occurred between 22 June and 12 July. The possible hydrological impacts of extreme melt events are therefore considered for periods prior to the initiation of subglacial outflow (early season, early–mid-June), around the time when subglacial outflow is initiated (mid-season, late June–early July), and when subglacial outflow is occurring (late season, mid-July to early August).

Given the normally low rates of early-season melt, especially at the UWS, extreme melt events at this time may increase the rate of snowline retreat on the lower glacier, lowering the snow albedo and possibly exposing the underlying ice surface. This would result in increased total seasonal melt, as the period for which low albedo ice was exposed would be increased. The impact of an early-season event on drainage development would, however, be limited by the need to warm the snowpack to 0 °C before melt can occur, and by the refreezing of meltwater within the snowpack, which delays runoff response (Fountain, 1996). Nevertheless, early-season events may have the effect of advancing the dates on which runoff and subglacial outflow are initiated.
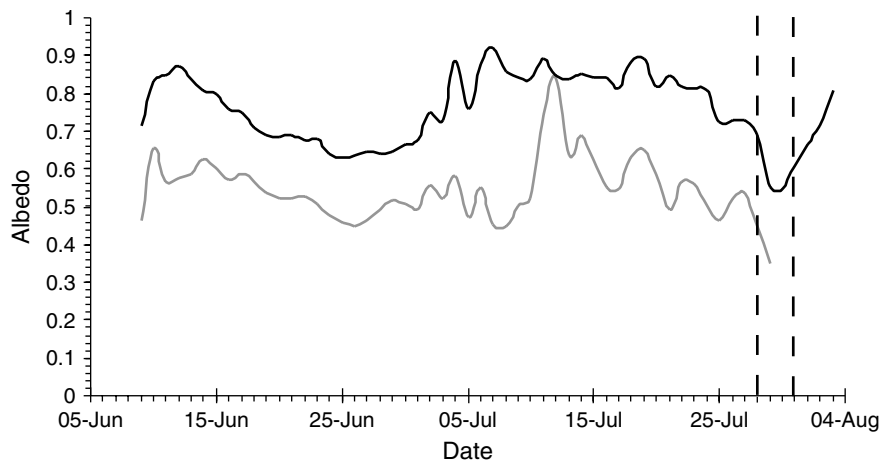
Figure 16. Measured albedo at the MWS (grey) and the UWS (black). The dashed lines mark the period of the event

By contrast, an event in late June or early July, when the snowpack had ripened and the surface albedo had dropped, could provide a major impetus for the establishment and initial growth of englacial and subglacial drainage passageways. This is significant, because July has the highest incidence of synoptic conditions similar to those that produced the event (Figure 14). The impact of such events on runoff may, however, be limited by the existence of a cold snowpack over much of the upper glacier at this time of year.

Late-season events would have a much stronger impact on runoff than events earlier in the season, but their influence on the development of englacial and subglacial drainage might be more limited. Low-albedo glacier ice melts rapidly under conditions such as those described, and the reduced snowpack later in the season would permit a more rapid runoff response (Fountain, 1996). However, it is likely that englacial and subglacial channels would already have formed in response to runoff earlier in the season, so the impact of large melt events could be limited to enlargement of pre-existing channels. In some cases, however, creation of new englacial connections between the supraglacial and subglacial systems might occur, resulting in upglacier expansion of the subglacial network (Nienow *et al*., 1998; Flowers and Clarke, in press).

In addition to their contribution to the development of drainage systems within glaciers, such events could play an important role in the ecology of subglacial and proglacial environments. The removal of the cryoconite layer could have important implications for the maintenance of life within and beneath glaciers. Cryoconites typically contain sediment, microbial populations, organic carbon, and nutrients (Vincent *et al*., 2000). On JEG, the organic carbon content of cryoconite sediment is typically 8–10% by weight. Thus, when transferred to the glacier bed, the contents of cryoconites could represent a source of innoculum, energy, and nutrients for subglacial microbial ecosystems, which are typically carbon and nutrient limited (Sharp *et al*., 1999; Skidmore *et al*., 2001). Sudden increases in the contribution of meltwater runoff to the discharge of glacier-fed rivers could result in noticeable lowering of stream temperatures, and expansion of the subglacial drainage network could enhance sediment transport, both of which may impact riverine ecology and benthic communities (McGregor *et al*., 1995).

Past events

The results presented above show that extreme events of short duration can make a disproportionate contribution to total summer melt, especially at high elevation sites that would normally be located in the accumulation area of the glacier. Although such events are rare, and no others occurred at JEG in the period 1996–2001, Keimig's synoptic database provides some evidence for clustering of similar events during some periods of the recent past. For instance, there were six events in the 1950s and nine in the 1980s, but only

six in the 1960s, 1970s and 1990s combined (Figure 15). Such changes in the occurrence of extreme melt events may contribute to both inter-annual variability and longer-term trends in seasonal runoff, drainage development, and glacier mass balance. The effect of such events is likely to be especially marked in the high Arctic, where both winter accumulation and summer melt are low, and inter-annual variability in summer mass balance is large. On the Devon and Meighen ice caps for instance, the coefficient of variation in summer mass balance is $\sim$70% (R.M. Koerner, unpublished data).

If major atmospheric oscillations (such as the Arctic oscillation or North Atlantic oscillation) or greenhouse-gas-induced climate warming resulted in systematic changes in the incidence of such events, this could be an important factor in determining the sensitivity of glacier mass balance to such changes. It is important, therefore, to establish whether the relationship between the incidence of synoptic configurations similar to those seen during the event, and larger-scale patterns of climate change and variability.

CONCLUSIONS

An extreme melt event occurred on JEG on 28–30 July 2000. As a result of the synoptic conditions associated with the event, airflow was routed over the northern sections of the Greenland Ice Sheet, resulting in strong northeasterly winds on the east coast of Ellesmere Island. Increased air temperatures and a sudden drop in relative humidity accompanied the strong winds at JEG.

The event had a significant impact on glacier melt, accounting for approximately 15% of total seasonal melt at the MWS, and 30% at the UWS. Enhancement of the melt rates was attributable largely to an increase in the turbulent heat fluxes, but at the UWS the contribution of net radiation to melt energy also increased due to snow-albedo feedback. The extreme melt event generated peak seasonal runoff, and removed the cryoconite layer from the surface of the glacier. Depending on the time of year at which such events occur, they may have a major impact on the timing and magnitude of summer ablation and runoff, the development of the englacial/subglacial component of glacier drainage systems, and the ecology of subglacial environments and glacially fed rivers. Variability in the occurrence of such events may also be a significant factor in the inter-annual variability and longer-term changes in the mass balance of high Arctic glaciers, and needs to be considered when evaluating the likely response of mass balance to climate change.

The synoptic conditions that created the event are rare, occurring on only 0·1% of days within the 1948–2000 record. They are, however, most common during the summer melt season, and were apparently more frequent in the 1950s and 1980s than in other recent decades. Given that such events can account for a large fraction of summer melt in a relatively short period, they may play an important role in determining the sensitivity of mass balance and runoff to climate changes. It is important, therefore, to investigate the relationship between the incidence of such events, longer-term climate trends and characteristic modes of climate variability.

REFERENCES

Arendt A. 1999. Approaches to modelling the surface albedo of a high Arctic glacier. *Geografiska Annaler A* **81**(4): 477–487.

Barry RG. 1992. *Mountain Weather and Climate*. Routledge Publishers: New York.

Brock BW, Arnold NS. 2000. A spreadsheet-based (Microsoft Excel) point surface energy balance model for glacier and snow melt studies. *Earth Surface Processes and Landforms* **25**: 649–658.

Copland L, Sharp M. 2001. Mapping hydrological and thermal conditions beneath a polythermal glacier with radio-echo sounding. *Journal of Glaciology* **47**: 232–242.

Courtin GM, Labine CL. 1977. Microclimatological studies on Truelove Lowland. In *Truelove Lowland, Devon Island, Canada: A High Arctic Ecosystem*, Bliss LC (ed.). University of Alberta Press: Edmonton; 73–106.

Doran PT, McKay CP, Adams WP, English MC, Wharton RA, Meyer MA. 1996. Climate forcing and thermal feedback of residual lake-ice covers in the high Arctic. *Limnology and Oceanography* **4**(15): 839–848.

Flowers GE, Clarke GKC. In press. A multicomponent coupled model of glacier hydrology: 2. Application to Trapridge Glacier, Yukon, Canada. *Journal of Geophysical Research*.

Fountain AG. 1996. Effect of snow and firn hydrology on the physical and chemical characteristics of glacial runoff. *Hydrological Processes* **10**: 509–521.

Gordon S, Sharp M, Hubbard B, Smart CC, Ketterling B, Willis I. 1998. Seasonal reorganization of subglacial drainage inferred from measurements in boreholes. In *Glacier Hydrology and Hydrochemistry*, Sharp M, Richards K, Tranter M (eds). John Wiley & Sons: Chichester; 239–267.

Heppenstall KE. 2001. *Chemical weathering in a glaciated carbonate catchment, Canadian high Arctic: implications for subglacial hydrology*. MSc thesis, University of Alberta.

Konzelmann T, Braithwaite R. 1995. Variations of ablation, albedo and energy balance at the margin of the Greenland ice sheet, Kronprins Christian Land, eastern north Greenland. *Journal of Glaciology* **41**(137): 174–182.

McGregor GR, Petts GE, Gurnell A, Milner AM. 1995. Sensitivity of alpine stream ecosystems to climate change and human impacts. *Aquatic Conservation: Marine and Freshwater Ecosystems* **5**: 233–247.

Nienow P, Sharp M, Willis I. 1998. Seasonal changes in the morphology of the subglacial drainage system, Haut Glacier D'Arolla, Switzerland. *Earth Surface Processes and Landforms* **23**: 825–843.

Paterson WSB. 1994. *The Physics of Glaciers*. Pergamon Press: Oxford.

Reeh N. 1991. Parameterization of melt rate and surface temperature on the Greenland Ice Sheet. *Polarforschung* **59**(3): 113–128.

Sharp M, Parkes J, Cragg B, Fairchild IJ, Lamb H, Tranter M. 1999. Widespread bacterial populations at glacier beds and their relationship to rock weathering and carbon cycling. *Geology* **27**: 107–110.

Skidmore ML, Sharp MJ. 1999. Drainage system behaviour of a high Arctic polythermal glacier. *Annals of Glaciology* **28**: 3–12.

Skidmore ML, Foght JM, Sharp MJ. 2000. Microbial life beneath a high Arctic glacier. *Applied and Environmental Microbiology* **66**: 3214–3220.

Vincent WF, Gibson JAE, Pieniitz R, Villeneuve V, Broady PA, Hamilton PB, Howard-Williams C. 2000. Ice shelf microbial ecosystems in the high Arctic and implications for life on Snowball Earth. *Naturwissenschaften* **87**(3): 137–141.